EUROFUSION WPMST2-PR(16) 15344

B Esposito et al.

Runaway generation and control

Preprint of Paper to be submitted for publication in
43rd European Physical Society Conference on Plasma
Physics (EPS)

This work has been carried out within the framework of the EUROfusion Consortium and has received funding from the Euratom research and training programme 2014-2018 under grant agreement No 633053. The views and opinions expressed herein do not necessarily reflect those of the European Commission.

Runaway Electron Generation and Control

B Esposito[1], L Boncagni[1], P Buratti[1], D Carnevale[2], F Causa[1], M Gospodarczyk[2], JR Martin-Solis[3], Z Popovic[3], M Agostini[4], G Apruzzese[1], W Bin[5], C Cianfarani[1], R De Angelis[1], G Granucci[5], A Grosso[1], G Maddaluno[1], D Marocco[1], V Piergotti[1], A Pensa[1], S Podda[1], G Pucella[1], G Ramogida[1], G Rocchi[1], M Riva[1], A Sibio[1], C Sozzi[5], B Tilia[1], O Tudisco[1], M Valisa[4] and FTU Team[1]

[1]*ENEA, Dipartimento FSN, C. R. Frascati, via E. Fermi 45, 00044 Frascati (Roma), Italy*
[2]*Dip. di Ing. Civile ed Informatica DICII, Università di Roma, Tor Vergata, Roma, Italy*
[3]*Universidad Carlos III de Madrid, Avda.Universidad 30, Leganes, 28911-Madrid, Spain*
[4]*Consorzio RFX, Padova, Italy*
[5]*IFP-CNR, Via R. Cozzi 53, 20125 Milano, Italy*

E-mail*: Basilio.Esposito@enea.it*

Abstract

We present an overview of FTU experiments on runaway electron (RE) generation and control exploiting a comprehensive set of real-time (RT) diagnostics/control systems and newly installed RE diagnostics (RE Imaging Spectrometer (REIS) system detecting visible and infrared synchrotron radiation, Cherenkov Probe measuring RE escaping the plasma, gamma camera providing Hard X-Ray radial profiles from RE bremsstrahlung interactions in the plasma). Experiments on the RE onset and suppression show that the threshold electric field for RE generation is larger than that expected according to a purely collisional theory, but consistent with with an increase due to synchrotron radiation losses. This might imply a lower density to be targeted with massive gas injection for RE suppression in ITER. Experiments on active control of disruption-generated RE, performed through feedback on poloidal coils by implementing a RT boundary-reconstruction algorithm evaluated on magnetic moments, indicate that the slow plasma current ramp-down and the simultaneous reduction of the reference plasma external radius are beneficial in dissipating the RE beam energy and population leading to reduced RE interactions with the plasma facing components, paving the way for an alternative or complementary technique to massive gas injection.

1. Introduction

Two important ITER physics issues concerning the control and mitigation of runaway electrons (RE) are addressed in this paper: the measurement of the threshold electric field for RE *generation* and the *active control* of position and current ramp-down of disruption-generated RE. FTU experiments in this field have been strongly supported by the recent integration of diagnostic, hardware and software tools in the real-time (RT) plasma control system. Several diagnostics used for RE measurements and control have been upgraded to RT operation and three new specific RE diagnostics have been installed: a) a Cherenkov probe detecting escaping fast electrons to study the RE dynamics in presence of magnetic islands [1]; b) a RE imaging system (REIS) to detect visible/infrared synchrotron radiation emitted by RE; c) an hard X-ray (HXR) radial profile monitor measuring in-plasma bremsstrahlung from RE [2].

2. Runaway Electron Diagnostics

A brief description of the diagnostic systems available for RE studies in FTU (R_0=0.935 m, a=0.3 m) is given below. More details can be found in the overview of the FTU diagnostics [3].

- *BF_3 chambers*: Six absolutely calibrated BF_3 proportional counters (5 ms integration time), only sensitive to neutrons, are placed in pairs on top of the cryostat [4] to monitor the neutron yield.
- *Fission chamber* (FC) - signal available in RT: The detector used in this study is a low sensitivity fission chamber manufactured by Centronic, with a coating of 30 $\mu g/cm^2$ of ^{235}U operated in pulse mode at 1 ms time resolution. During the RE plateau phase the FC measures photoneutrons and photofissions induced by gamma rays (with energy higher than ~7 MeV) produced by thick-target bremsstrahlung (RE interacting with the metallic plasma facing components (PFC)).
- *NaI scintillator* - signal available in RT: 3" diameter x 3" thick, coupled to a photomultiplier (PMT), sensitive to Hard X-Rays (HXR) with energy > 200 keV mainly emitted by RE hitting the vessel, operated in current mode (1 kHz sampling rate), viewing the plasma on the equatorial plane (signal labelled as HXR in the figures). It also works as spectrometer up to ~20 MeV with 100 ms time resolution [5].

- *NE213 organic liquid scintillator*: 5" diameter x 5" thick, coupled to a PMT, sensitive both to neutrons and HXR, operated in current mode (20 kHz sampling rate), placed without any collimation on the equatorial plane outside the cryostat and cross calibrated with the set of BF_3 neutron detectors in discharges with no RE [5]. The NE213 detector is used to monitor the HXR emission from in-plasma bremsstrahlung of REs and/or bremsstrahlung due to RE interactions with the PFCs. However, in the disruption and RE plateau phases, the NE213 usually saturates and its monitor role is taken over by the FC (see below).
- *Gamma camera*: The FTU neutron camera [6] has been optimized for RE studies through a digital upgrade (14-bit, 400 MSamples/s) of its acquisition system [7]. It has six collimated Lines Of Sight (LOS), viewing the plasma from a lower vertical port; each LOS is equipped with a NE213 detector (2" diameter x 2" thick) coupled to a PMT and an embedded ^{22}Na source for calibration purposes. The detectors are capable of n/γ discrimination, operated in count mode and sensitive to HXR with energy >100 KeV. The gamma camera provides radially resolved measurements of HXR emitted perpendicularly to the magnetic field and produced by RE through bremsstrahlung in the plasma, with a time resolution, depending on the count rate, down to ~1 ms [2].
- *Fast Electron Bremsstrahlung (FEB) camera*: The camera has horizontal and vertical lines of sight (5 ms integration time) and detects HXR emission in the energy range 20-200 keV by means of cadmium telluride semiconductors [5].
- *Soft X-Ray pinhole camera*: Soft X-Rays (SXR) in the range of 1 keV to 15 keV are detected by a set silicon PIN diodes with a large number of collimated lines of sight distributed on two cameras (44 vertical and 68 horizontal LOS in a poloidal cross-section) [3].
- *Runaway Electron Imaging and Spectrometry (REIS) system*: A wide-angle optical system collects the RE synchrotron radiation from two plasma cross sections (corresponding respectively to the RE backward and forward view) and transmits it to visible/infrared spectrometers through an incoherent bundle of fibres (**Figure 1**); the spectral range spans from 300 to 2100 nm.

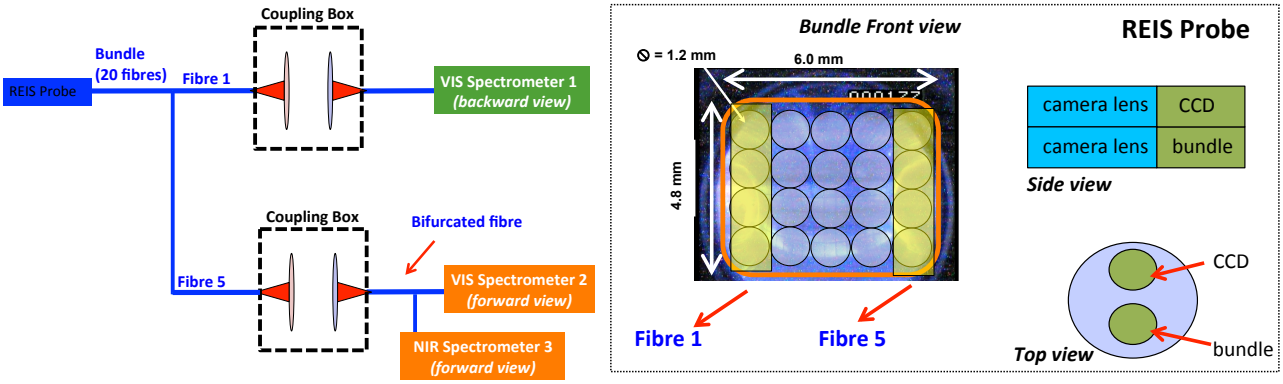

Figure 1. *Layout of Runaway Electron Imaging and Spectrometry (REIS) system*

- *Cherenkov Probe*: It consists of a single-crystal diamond detector (10 mm diameter, 1 mm thickness) mounted on a titanium zirconium molybdenum (TZM) head inserted into the FTU vessel [1]. The detector is coated with a 100/200/1000 nm Ti/Pt/Au interlayer filtering out visible light, particularly the plasma Dα line. Electrons impinging on the probe emit Cherenkov radiation in diamond if $v>c/n_d$ (v=electron speed, c=speed of light, n_d=refractive index of diamond), a condition corresponding to 58 keV electron energy threshold. The Cherenkov radiation is routed, through a visible/ultraviolet optical fibre, to a PMT operating in the 160– 650 nm spectral range. The time resolution is 1 μs.
- *CO_2/CO two-color scanning interferometer* - signals available in RT: It provides the number of electrons measured on several plasma vertical chords intercepting the equatorial plane at different radii ranging from 0.8965 m to 1.2297 m with a sampling time of 62.5 μs. The electron density profiles are produced through a radial inversion technique [3]. Detailed information related to mounting position and specific features are given in [8]. The RT processing of electron density data from the CO_2/CO interferometer has recently been carried using the MARTe (Multi-threaded Application Real-Time executor) framework running under a Linux operation system installed on a Compact PCI multicore system [9]. The industrial

controller is equipped with three high-speed acquisition boards (maximum sampling rate 2.0 MHz) and one reflective memory to share data with the FTU RT network.

- *MHD sensors* - signal available in RT: The plasma magnetic activity is monitored by means of a set of poloidal field pick-up Mirnov coils. The amplitude of the Mirnov coil signals is directly related to helical deformations of the plasma resulting from MHD instabilities, having in most cases n=1 (m=2) toroidal (poloidal) periodicity.

RE in flight in the plasma are detected by measuring SXR radiation, HXR bremsstrahlung, and infrared/visible synchrotron radiation, while RE that have escaped the plasma are measured by direct fast electron loss and gamma rays from thick target bremsstrahlung on plasma facing components (together with the corresponding neutrons produced in photonuclear reactions (γ, n)).

3. Runaway Electron Dynamics

The FTU RE diagnostics provide information on various features of the RE dynamics:

- *Spatial localization*: Radial profiles of HXR indicate that, in general, RE are initially produced in the centre of the plasma (see also [2]). **Figure 2** provides an example: in discharge #39469 the appearance of RE is characterized by a peaked profile of the HXR line-integrals (t~0.65s) **(right)**; subsequently, as RE gain energy, as also shown by the rise of the photoneutron emission starting at t~0.85s **(left)**, the HXR emission peaks off-axis as a result of the RE radial losses and outward orbit drift.
- *Energy*: Past FTU measurements (HXR spectra from the NaI scintillator) have shown RE energies up to ~20 MeV [5]. Novel measurements from the REIS diagnostic indicate even higher energies, in excess of 30 MeV. **Figure 3** (discharge #39516) shows images of the RE beam from the visible camera correlated with the measured synchrotron radiation intensity at several wavelengths **(right top)** and the measured synchrotron radiation visible spectra **(right bottom)**. The spectra are fitted (black solid lines) using formula (1) from [10] for a monoenergetic distribution. The measured energy and picth angle values (see insert in **Figure 3(right bottom)** are in agreement with the predictions of simulations based on a test particle model of the RE dynamics [11]: in #39516 RE form already at ~0.05s, as shown (**Figure 4(left)**) by the offset between the NE213 and BF_3 time traces **(top)** and the calculated Dreicer RE birth rate (secondary RE generation can be neglected in FTU) **(middle)**. The calculated RE energy distribution (**Figure 4(right)** gradually becomes monoenergetic with a maximum energy of ~30 MeV (**Figure 4(left bottom**)).
- *Losses:* Loss of RE from the plasma, often in correspondence with MHD events, is directly measured by the Cherenkov probe. An example is shown in **Figure 5** where phase-relations between Cherenkov, ECE and neutron (NE213 and BF_3) signals show that the modulation of the Cherenkov signal associated with local RE losses is due to the magnetic island rotation [1].

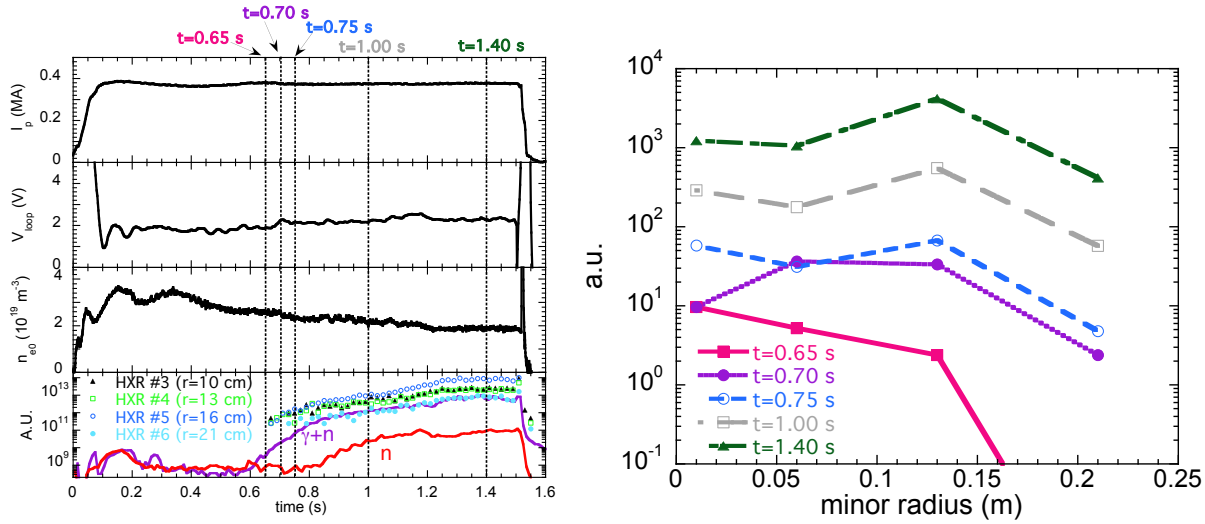

***Figure 2**. Discharge 39469 (B_t=4.1 T). (a) Time traces of plasma current (I_p), loop voltage (V_{loop}), line-averaged electron density (n_e), line integrated HXR from gamma camera, HXR from NE213 scintillator and neutrons from BF_3. (b) Radial profiles of line-integrated HXR emission from RE.*

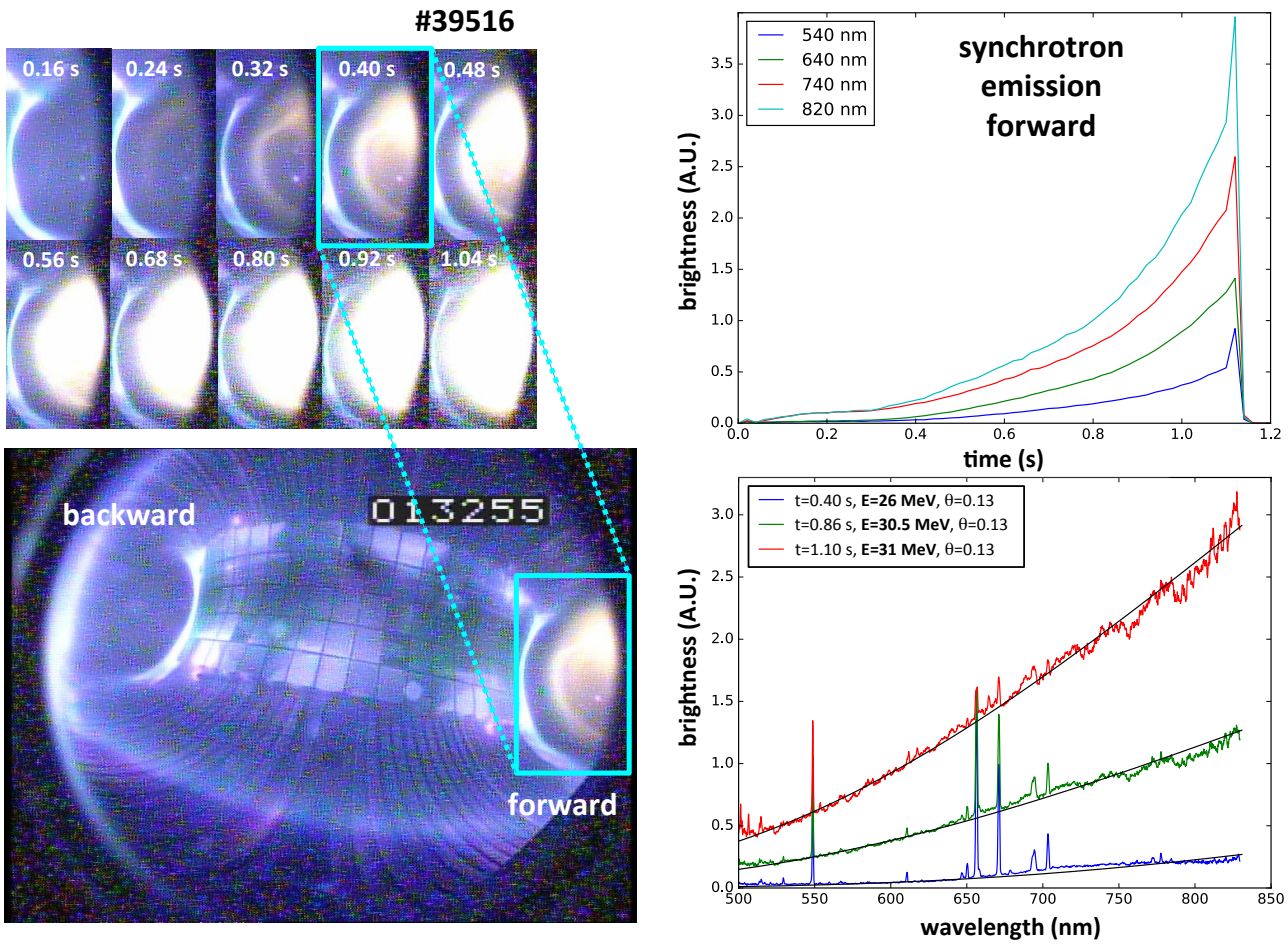

Figure 3. *Discharge #39516 (B_t=3.7 T): Visible camera images (forward view) of the RE beam* ***(left)*** *correlated with measured synchrotron radiation intensity at several wavelengths* ***(right top)*** *and synchrotron radiation visible spectra* ***(right bottom)***. *The spectra are fitted (solid lines) assuming monoenergetic distributions (energy and pitch angle values in the insert).*

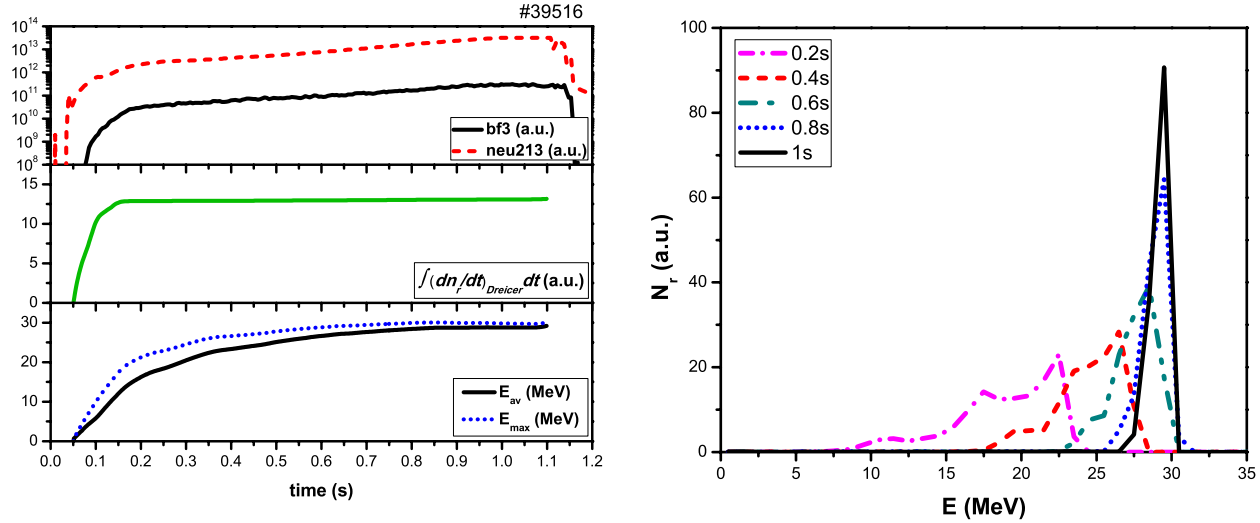

Figure 4. *Discharge #39516 (B_t=3.7 T). (left) Time traces of BF_3 and NE213 signals (top), calculated Dreicer birth rate (middle) and calculated average and maximum energy (bottom). (right) Calculated RE energy distributions.*

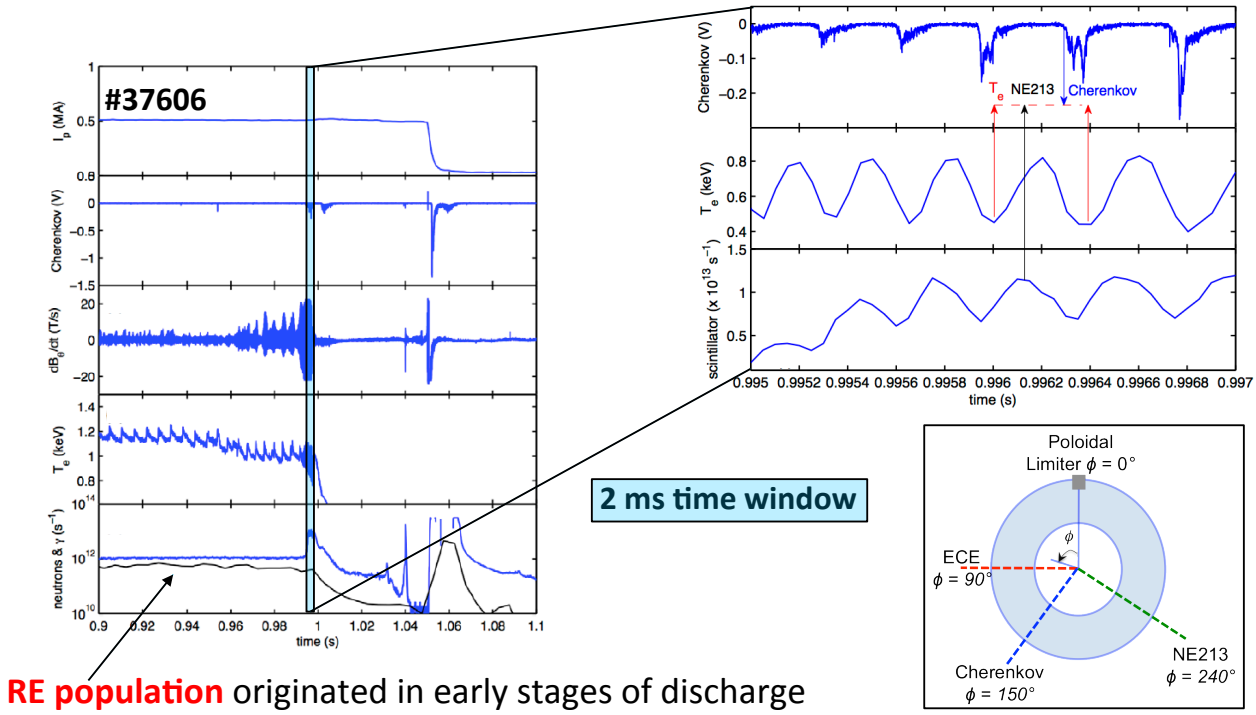

Figure 5. *Discharge #37606 (B_t=5.3 T): Correlation between Cherenkov probe, ECE and NE213 signals showing loss of RE during MHD activity.*

4. Runaway Electron Generation

RE represent a major threat in the operation of tokamaks, especially when generated in a disruption, and the understanding of the conditions that lead to their generation are important in the design of systems (such as massive gas injection (MGI)) dedicated to their suppression.

The relativistic collisional theory of RE generation [12] predicts that no REs can be generated below a critical electric field (E_R) determined from the balance between electric field acceleration and collisional damping:

$$E_R = \frac{n_e e^3 \ln\Lambda}{4\pi\varepsilon_0^2 m_e c^2} \qquad (1).$$

Hence, the necessary condition for RE avalanche growth is that the acceleration due to the toroidal electric field has to be higher than the collisional drag on the background particles, $E>E_R$. E_R scales linearly with the electron density n_e. The method adopted by the disruption mitigation system being designed for ITER to suppress the RE avalanche growth is to raise n_e sufficiently high: however, the large quantity of injected gas may be problematic for the subsequent machine operation.

There are various indications that other RE loss mechanisms may exist in addition to collisional damping:

a) The electron synchrotron radiation losses (neglected in the theory above) has been found to play an important role in RE suppression experiments by means of electron-cyclotron-resonance heating during the flattop phase of FTU discharges [13]. It has been observed that RE suppression occurs at electric fields substantially larger than those predicted by the relativistic collisional theory of runaway generation. The experimental results are consistent with an increase of E_R due to the electron synchrotron radiation, which lead to a new electric field threshold E_R^{rad} [13]:

$$\frac{E_R^{rad}}{E_R} \cong 1 + C(Z_{eff})\, F_{gy}^{\alpha} \qquad (2)$$

where

$$\alpha = 0.45 \pm 0.03; \quad F_{gy} \equiv \frac{2\varepsilon_0 B_0^2}{3 n_e \ln\Lambda m_e}; \quad C(Z_{eff}) \cong 1.64 + 0.53\, Z_{eff} - 0.015\, Z_{eff}^2 \qquad (3).$$

b) Data from the ITPA joint experiment to study RE generation and suppression in several tokamaks [14]

show that the measured threshold electric field for RE generation (E_{thr}) is 3–5 times higher than E_R, which, in turn, means that RE should be mitigated at densities lower than predicted.

The results of the systematic investigation of the conditions for RE generation in the plasma current (I_p) flattop phase of FTU deuterium ohmic discharges are reported here. E_{thr} has been evaluated in two different types of experiments: 1) *RE onset*; 2) *RE suppression*.

Figure 6 shows the time traces of I_p, loop voltage (V_{loop}), BF_3 chambers and NE213 scintillator signals and the central line-averaged electron density ($\bar{n}_{e0}$) for a *RE onset (left)* and a *RE suppression (right)* experiment. The *RE onset* is obtained through a decreasing electron density (n_e) in the I_p flattop. The *RE suppression* is achieved by starting a discharge with low gas prefill thus creating a RE population subsequently suppressed by a feedback-controlled phase of constant or increasing n_e. The time of *RE onset/suppression* is determined through the comparison of the time traces of the BF_3 and NE213 signals. In the *RE onset* experiments, during the pre-RE phase the NE213 signal overlaps with the BF_3 signal, while, as soon as the REs are generated, the two time traces diverge. On the other hand, in the *RE suppression* experiments, the NE213 signal is higher in the initial phase, indicating presence of RE, while later on, when *RE suppression* occurs, the two signals coincide. The time of the *RE onset/suppression* (t_c in the figures) is obtained by calculating the difference between the logarithms of the BF_3 and NE213 signals normalized to the NE213 signal and comparing it with the baseline value before the REs set in or after they disappear; the threshold field is then estimated as $E_{thr} \sim \frac{V_{loop}(t_c)}{2\pi R_0}$. Note that there is an instrumental limit for the minimum amount of RE that can be detected and this depends on the detector sensitivity: therefore, for example, some RE may be already present in the plasma while the BF_3 and NE213 signals still coincide. However, the use of two separate methods (*RE onset* and *suppression*) gives us the possibility to determine respectively an *upper* and *lower* limit for E_{thr}.

The parameter space investigated in the experiments is highlighted by the three plots in **Figure 7**, which shows the range of measured E_{thr} values as a function of I_p, toroidal magnetic field (B_t) and effective charge (Z_{eff}) respectively. Each point corresponds to a different discharge. The database spans a wide range of plasma parameters: B_t=2-7.2 T, I_p =0.35-0.9 MA and Z_{eff}=1.5-13.

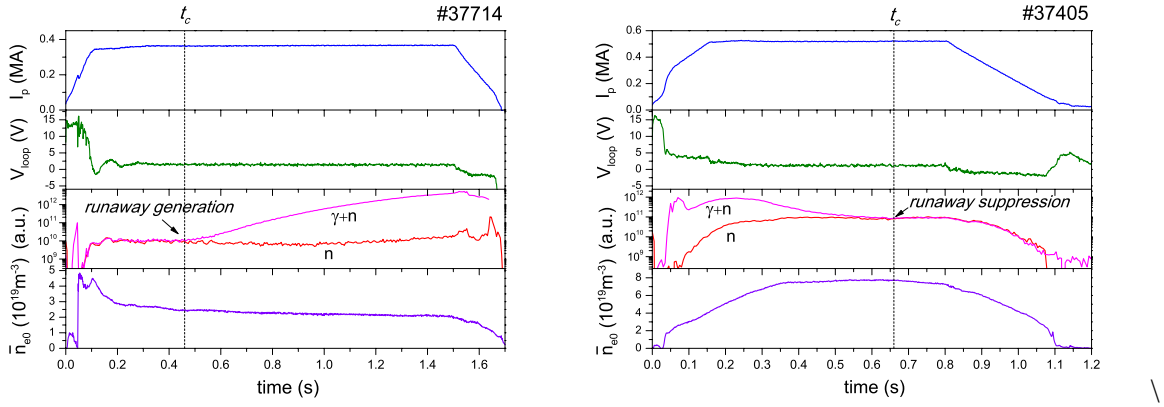

***Figure 6**. RE onset and suppression: time traces of I_p, V_{loop}, NE213 (γ+n) and BF_3 (n) signals and line-averaged central density.*

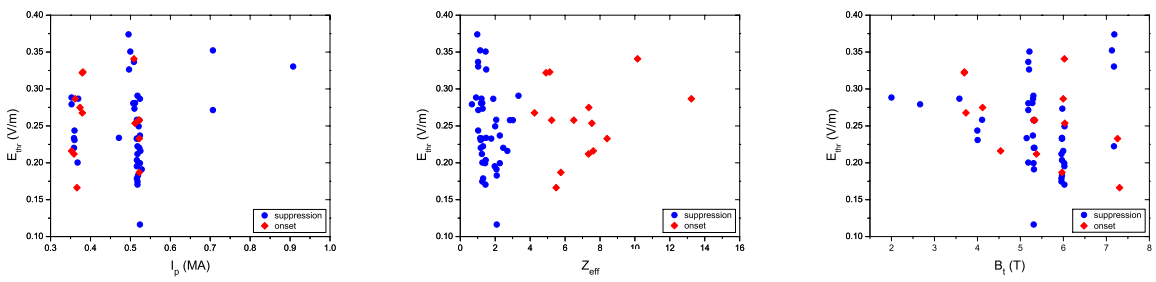

Figure 7. *Parameter range in the RE onset/suppression experiments.*

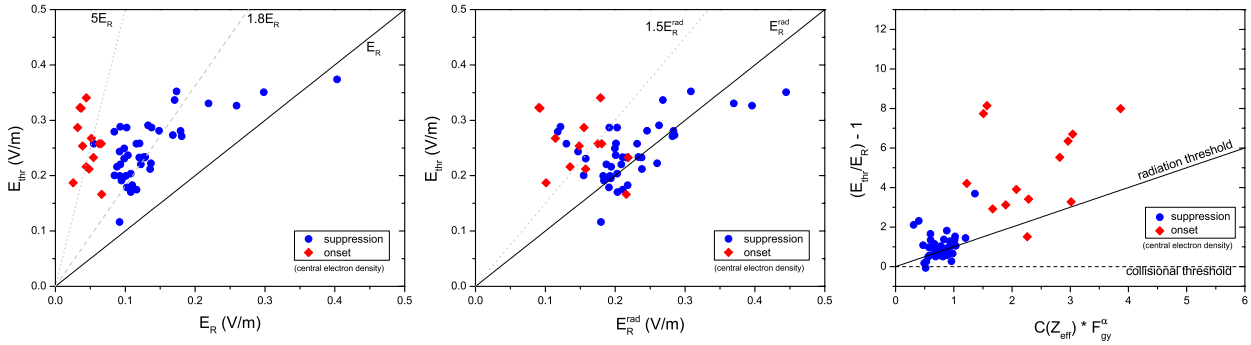

***Figure 8**. Comparison of measured E_{thr} with: (left) relativistic collisional radiation theory predictions (E_R); (centre) relativistic collisional+synchrotron radiation theory predictions (E_R^{rad}).*

The measured E_{thr} values have been compared with the predicted E_R and E_R^{rad} (evaluated using the local central electron density n_{e0}, instead of the line-averaged central density $\bar{n}_{e0}$, as it provides a better match with the experimental data). The plots of **Figure 8(left)** and **(center)** indicate that the measured E_{thr} is ~2-5 times larger than the threshold electric field, E_R, predicted by the classical collisional theory [12] while it is consistent with the new threshold calculated including synchrotron radiation losses [13]. In addition, the dependence of on the plasma parameters predicted by the synchrotron radiation theory (relations (2) and (3)) reasonably agrees with E_{thr}, as illustrated in **Figure 8(right)**.

5. Runaway Electron Control

A crucial challenge towards a safe and efficient operation of ITER consists in the reduction the dangerous effects of RE during disruptions [15]. RE are considered to be potentially intolerable for ITER when exhibiting currents larger than 2 MA. The main strategy to address this problem is RE suppression by means of MGI of High-Z noble gas before the thermal quench (TQ), which has the additional advantage of reducing the localized heat load. However, MGI leads to long recovery time, requires effective disruption predictors, and may lead to hot tail RE generation [16] or high mechanical loads if the Current Quench (CQ) does not occur in a suitable time interval [15, 17, 18]. In any circumstance in which such suppression strategy may not be effective, for instance due to a delayed detection of the disruption and/or to a failure of the gas valves or of disruption avoidance techniques (e.g. using ECRH [19]) alternative RE mitigation strategies may be pursued, such as *Resonant Magnetic Perturbations* to suppress RE [20, 21, 22], however requiring specific active coils that are not available in FTU, and *RE active control* to dissipate the RE beam energy and population [23, 24, 25].

We present here FTU results on *RE active control*, i.e. stabilization of the disruption-generated RE beam by minimizing its interaction with the PFC) The RE energy dissipation is obtained by reducing the RE beam current via the central solenoid (inductive effects). In particular, the focus here is on those RE that survive the CQ. When the RE beam position is stabilized, further techniques, not studied in the present paper, such as high-Z gas injection to increase RE beam radiative losses could be exploited.

In the last years, experiments on *RE active control* have been carried out in DIII-D [23], Tore Supra, FTU, JET, and initial studies have been carried out also at COMPASS [26]. In Tore Supra attempts of RE thermalization via MGI (He) have been investigated [27]. In DIII-D disruptions have been induced by injecting either Argon pellets or MGI while the ohmic coil current feedback has been left active to maintain constant current levels or to follow the reference current ramp-down [23]. DIII-D also studied the current beam dissipation rate by means of MGI with a final termination at approximately 100 kA [28]. Similar results on MGI mitigation of RE have been obtained at JET [29]. The present work goes along similar lines, but the RE beam dissipation is obtained only by inductive effects, i.e. via central solenoid as in [23], combined with a new dedicated tool of the FTU Plasma Control System (PCS). This scheme provides a RE beam current ramp-down and position control. The effectiveness of the novel approach is measured in terms of reduced interaction of RE with the PFC.

Two novel real-time (RT) algorithms (*PCS-REf1* and *PCS-REf2*) for position and I_p ramp-down control of disruption-generated RE have been developed, implemented within the framework of the FTU PCS and tested in dedicated FTU plasma discharges. The active coils used to control the position and the current of the plasma are shown in **Figure 9**.

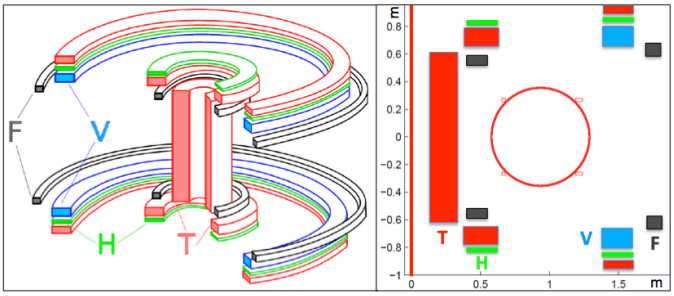

***Figure 9**. Active FTU coils. T controls the plasma current, V and F the plasma column radial movements and elongation, H the plasma column vertical position.*

The FTU PCS, extensively described in [30], exploits the current flowing within the T coil, called the central solenoid, to impose I_p via inductive effect. The T coil current I_T is regulated via a feedback control scheme based on a Proportional-Integral-Derivative (PID) regulator, which is driven by the I_p error plus a pre-programmed signal. The horizontal position of the plasma is controlled by means of an additional PID regulator that is fed with the horizontal position error. Such error is obtained by on-line processing of a series of pick-up coil signals to determine the plasma boundary (last closed magnetic surface) which is compared along the equatorial plane to the reference plasma internal R_{int} and external R_{ex} radii, (see [31, 32, 33, 34] for further details). The current flowing in the F coil (I_F), by geometrical construction, allows us also to modify the plasma elongation ε. The current in the V coil (I_V), which produces a vertical field similar to F but with a slower rate of change, is modified by a specific controller (Current Allocator [35]) in order to change at run-time I_F and maintain unchanged the vertical field. In such a way, the plasma radial position is left unchanged and at the same time it is possible to steer the value I_F away from saturation levels. The current redistribution (reallocation) between I_F and I_V is performed by the Current Allocator at a slower-rate than the changes imposed on I_F by the PID regulator (PID-F) for plasma horizontal stabilization. The PCS safety rules impose that whenever the HXR signal takes values above a given safety threshold for more than 10 ms, indication that harmful RE are present, the discharge has to be shut-down. In the *Standard* shut-down control algorithm the I_p reference is exponentially decreased down to zero and the reference inner and outer plasma radii at the equatorial plane (R_{int} and R_{ext}) are left unchanged.

PCS-REf1 has been specifically designed for RE beam dissipation and comprises two different phases. In the first phase, specific algorithms described in [35] are employed to detect the CQ and the RE beam plateau by processing the I_p and the HXR signal. At the same time, the Current Allocator steers the values of I_F away from saturation limits, to ensure that a larger excursion is available for the control of the RE beam position. In the second phase, once the RE beam event has been detected (CQ or HXR level), the I_p reference is linearly ramped-down in order to dissipate the RE beam energy by means of the central solenoid. A scan of the initial values and slope of the updated I_p reference for RE suppression (current ramp-down), that substitutes the standard I_p reference when the RE beam is detected, has been performed. At the same time, the reference external radius R_{ext} is reduced linearly with different slopes down to predefined constant values. R_{ext} is reduced in order to compensate for a large outward shift of the RE beam, hence to preserve the low field side vessel from RE beam impacts. The reduction of the R_{ext} reference can be considered the way of finding the RE beam radial position that provides minimal RE beam interaction with PFC: similar findings have been discussed in [23] and the RE beam position with minimal PFC interaction is called the "safe zone". In all the experiments, the reference R_{int} is not changed since plasma operation is in (internal) limiter configuration. Nevertheless, the control system has the objective to maintain the plasma within the reference horizontal and vertical radii, avoiding the plasma impact with the vessel (both sides).

PCS-REf2 has been designed with the same objective (RE beam control and energy suppression) as *PCS-REf1*. The main difference consists in the fact that the updated reference R_{ext} is ramped-down to a specific constant value (within the range 1.11-1.13 m) associated to a reduced level of the FC signal (as experienced in the experiments in which PCS-REf1 was active) plus a small time-varying term. Such term (constrained to belong to the range [-0.04,0.04] m), is computed in real-time by processing the measured R_{ext} and FC signals according to the extremum seeking technique (similar to a gradient algorithm discussed in [36, 37]) in order to minimize the RT FC signal. Furthermore, the I_p ramp-down slope selected for *PCS-REf2* is about three times smaller than in *PCS-REf1*.

Due to the current amplifiers limitations, *PCS-REf1* and *PCS-Ref2* are not expected to be effective in position and I_p current ramp-down control within 25-30 ms of the CQ detection.

The two new RE active control algorithms have been tested in dedicated RE deuterium discharges. *PCS-Ref1* has been applied in a RE scenario in which a significant RE population is generated during the I_p ramp-up/flat top (360 kA, 6T) by using a low gas prefill and a low density reference ($1.5x10^{19}$ m^{-3}), followed by an injection of neon gas to induce a disruption (*RE Scenario 1*). The sudden variation of the resistivity and the increased loop voltage at the disruption accelerate the pre-existing RE population and lead, in some cases, to the formation of a RE current plateau which is the target scenario of these experiments. Note that this scenario is not a method to create runaways but to turn an existing seed population of RE in a runaway plateau at the disruption. The discharge is run with an initial low gas prefill in such a way that early in the discharge ramp up a runaway population is established. *PCS*-REf2 has been tested in a RE scenario differing from the first one because of the use of an even lower gas prefill, which causes spontaneous disruption during the I_p ramp-up and, again, in some cases, a RE plateau (*RE Scenario 2*).

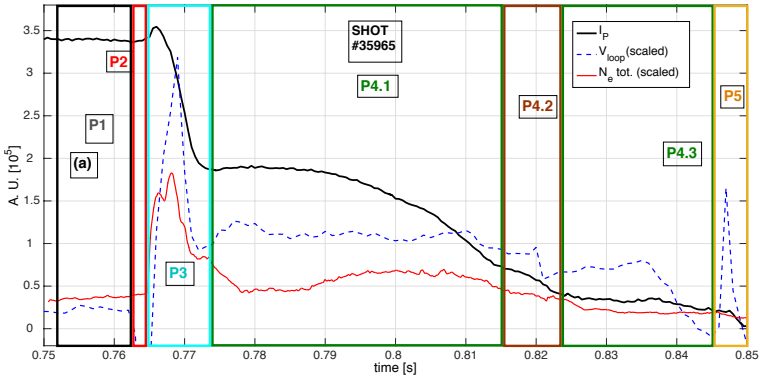

***Figure 10**. Discharge #35965: plasma/RE current (black), total number of electrons computed from CO2 interferometer (red solid), loop voltage (dashed blue). The different phases (P1 to P5) are highlighted.*

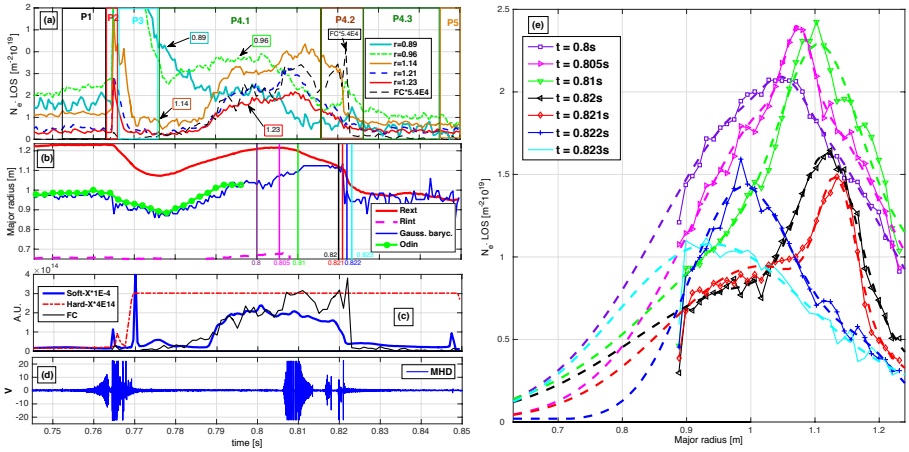

Figure 11. Discharge #35965: (a) CO2 interferometer electron density line integrals compared with the FC signal (black dashed); (b) R_{ext} (red solid), R_{int} (pink dashed), $R_{ne\ max}$ (black), R_{mag} (green); (c) signals of SXR central line of sight (blue), HXR monitor (red), FC (black); (d) Mirnov coils; (e) radial profiles of electron density line integrals (solid=raw data, dashed= fitted data).

The characterization of the different phases of a disruption with the generation of a RE plateau is given in **Figure 10** for a typical discharge of *RE scenario 1*. After Ne gas injection, the plasma density slightly increases during the pre-disruptive phase P1. The TQ (phase P2), lasting few milliseconds (1-2 ms), in which the plasma confinement is lost and the thermal energy is released to the vessel combined with the high electrical field, produces a large increase of the electron density. The CQ phase P3 follows: it is characterized by a sudden drop I_p and a high self-induced parallel electric field (V_{loop}) that further accelerates the pre-existing RE and possibly increases their number. The RE plateau phase (P4) follows and can be, in turn, divided into three sub-phases: in phase P4.1 the RE beam current exponentially replaces a large fraction of the ohmic I_p current (see [28], this process starts with the onset of the CQ); subsequently, part of such current can be lost due to instabilities (P4.2), while the rest of the beam can survive (further plateau in phase P4.3) before the final loss (phase P5).

Figure 11 shows the time traces of some of the CO2 interferometer electron density line integrals **(a)** and the radial profiles of these integrals at different times **(e)**. Note that the line integrals are available only in the range from 0.8965 m to 1.2297 m. The radial profiles of the line integrals have been fitted with Gaussian functions (least square minimization) in order to compute, by integration over the major radius R and toroidal angle, the total number of electrons (N_e) and the major radius corresponding to the density peak ($R_{ne\ max}$), as shown in panel **(b)**: such figure also shows the radius of the magnetic axis as reconstructed by the ODIN equilibrium code (R_{mag}), and the experimental inner and outer plasma radii at the equatorial plane from magnetic measurements (R_{int} and R_{ext}). Finally, panels **(c)** and **(d)** show respectively the signals form the X-ray monitors and MHD coils.

The time traces of some of the CO2 interferometer electron density line integrals in the time interval between the RE plateau onset (~ 0.775 - 0.82 s) show that the cold plasma column is moving towards the low-field side: correspondingly, the FC signal increases due to the increased RE loss onto the outer limiter (phase P4.1). A large outer shift and an extremely peaked profile of the cold plasma column can be seen at approximately 0.81 s. An outward shift of the RE beam orbits is indeed a well known feature of the RE beam [23]. The RE beam is therefore centred on the right of $R_{ne\ max}$, although it is not possible to determine its position exactly.

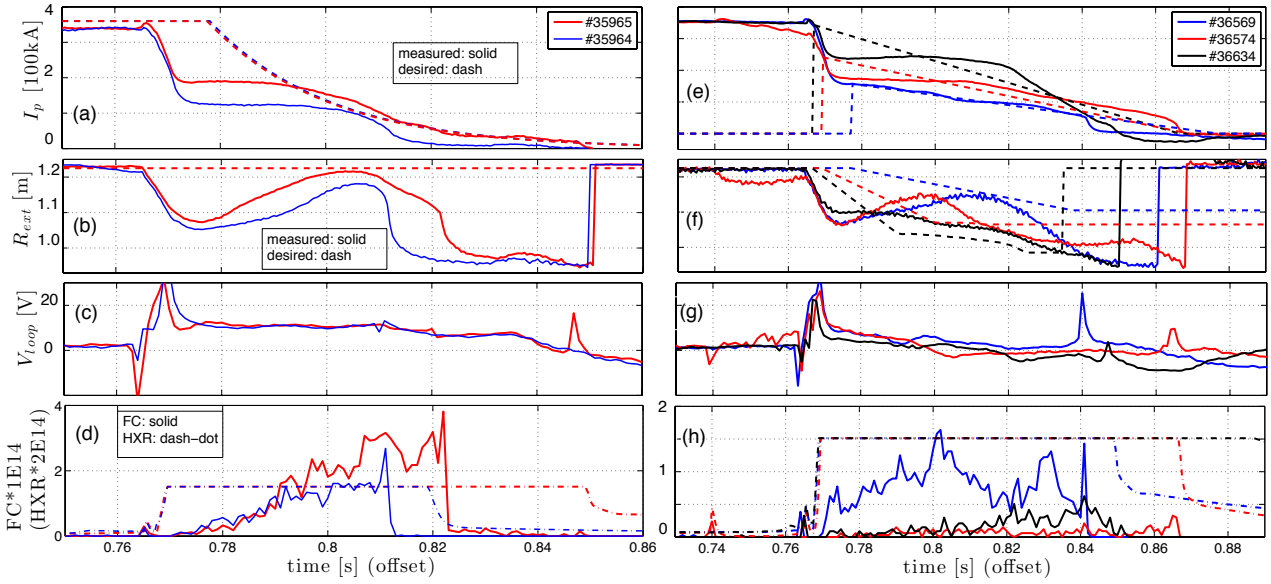

Figure 12. Scenario 1 (see text for details): (left) No runaway control (*Standard algorithm*); (right) Runaway active control (*PCS-Ref1 algorithm*).

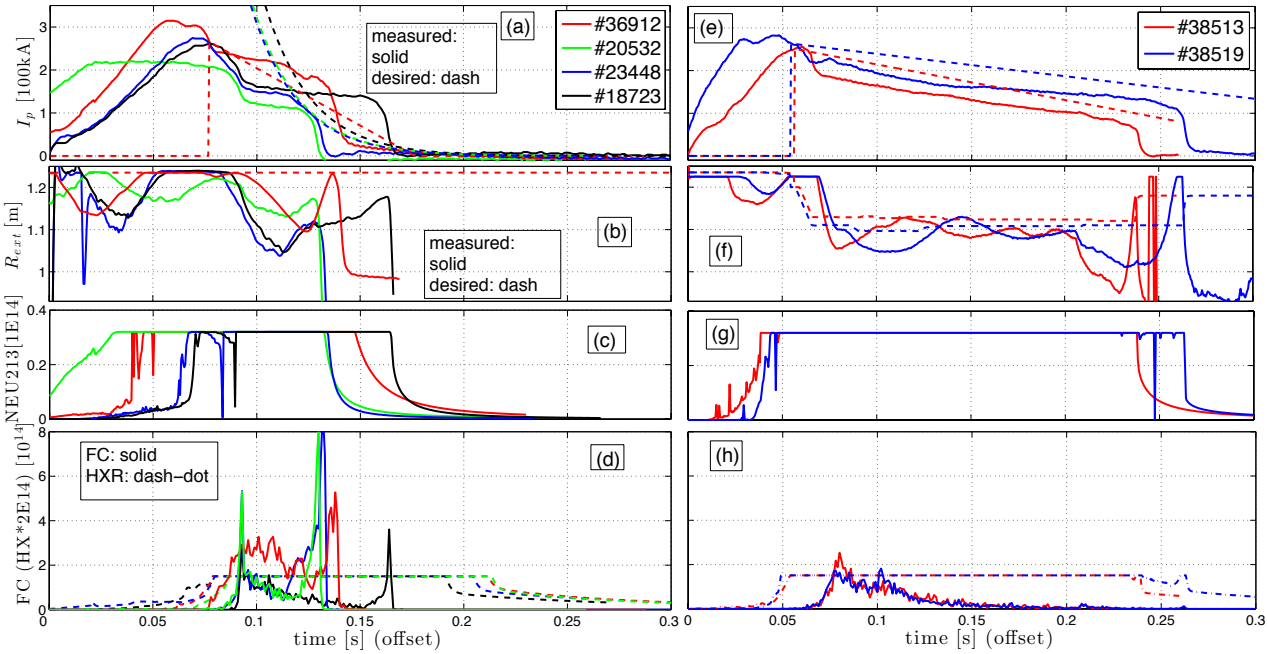

Figure 13. Scenario 2 (see text for details): (left) No runaway control (*Standard algorithm*); (right) Runaway active control (*PCS-Ref2 algorithm*).

The *PCS-REf1* and *PCS-Ref2* RE active control results in *RE Scenario* 1 and *RE Scenario 2* are shown in **Figure 12** and **Figure 13**, respectively. The I_p reference at flat top is typically 360 kA (500 kA for discharges #20532, #23448, #18723). The control algorithms replace the I_p reference by a linear ramp-down as shown by the dashed lines in panel **(e)**. Panels **(b)** and **(f)** show the measured (solid) and reference (dashed) R_{ext}. R_{ext} is kept constant (1.23 m) in the *Standard* control algorithm, whereas in *PCS-REf1/2* is changed dynamically at run-time. The following other signals are shown: V_{loop} in panels **(c)** and **(g)**, FC (solid) and HXR (dashed) in panels **(d)** and **(h)**, NE213 scintillator in panels **(i)** and **(l).**

5.1 RE Scenario 1 / PCS-REf1

The start of the I_p ramp-down has been varied in different pulses by modifying specific parameters of the CQ detector, whereas the ramp-down slopes have been set directly modifying the controller configuration file. The new I_p reference allows us to define an updated I_p error that is fed to the PID-T controller. The PID-T acts on a current amplifier in order to change the current flowing within the central solenoid I_T, thus obtaining a RE beam current suppression by induction. The new I_p reference ramp-down induces a lower V_{loop} than in the standard case (**Figure 12(c),(g)**), due to the action of the control system that modifies the rate of the current in the central solenoid coil, hence reducing the energy transferred by the central solenoid to the RE and, consequently, reducing also the RE radial outward shift. On the contrary, in the *Standard* control algorithm the effort of the PCS to recover the flat-top I_p value induces large voltages that increase the RE energy and also their outward shift. Simultaneously, the smaller new R_{ext} reference contributes to the reduction of the RE beam interaction with the low-field side wall. The improvement of *PCS-REf1* discharges in terms of reduced FC signal is quite evident (note the different scales in the FC panels), especially for discharges #36574 and #36634 where R_{ext} is reduced of more than 10% with respect to the standard value.

5.2 RE Scenario 2 / PCS-Ref2

The controller is not activated by the detection of the CQ or current plateau onset, as in *Scenario 1*, but when the HXR signal exceeds the safety threshold. Both hard x-rays monitors (NE213 and HXR) are saturated since the CQ throughout the I_p ramp-down indicating that energetic RE are present. R_{ext} is set to an initial value but, afterwards, is adjusted in RT: the RT FC signal is exploited to slightly modify R_{ext} and minimize the FC signal itself. Note the sudden ramp down of R_{ext} to 1.11 m and 1.13 m, respectively, in discharges #38519 and #38513 and the subsequent slight changes in time. The following improvements are observed when using *PCS-Ref2*:

- discharges with *RE active control* show a reduction of the FC signal down to zero during the slow I_p ramp-down and R_{ext} decrease, while those with no *RE active control* disrupt earlier and show a large FC final peak at the RE loss;
- despite the larger RE beam final current loss in *PCS-REf2* with respect to *PCS-Ref1* the corresponding final FC peaks are noticeably smaller, almost negligible;
- the HXR signal drops below the saturation value before the final loss in #38519 unlike the other discharges: since the current drop at the final loss is about 100 kA, this may suggest that a considerable RE beam energy has been dissipated (electron thermalization) during the I_p ramp-down;
- the use of a R_{ext} RT reference constrained by the FC RT signals seem to improve the capability of the control to maintain the RE beam for longer time intervals than in *PCS-Ref1* (up to 200 ms).

The *PCS-Ref1/2* results suggest the importance of reducing the external plasma radius reference to minimize the RE interactions with the vessel, confirming similar results discussed in [23].

6. Conclusions

The RE energy and pitch angle inferred from spectral synchrotron radiation measurements of the novel RE imaging and spectrometry (REIS) diagnostic installed in FTU are found to be consistent with the predictions of a test particle model of the RE dynamics. Energy values up over 30 MeV and pitch angles of the order of 0.1 rad have been measured. HXR profile measurements of RE bremsstrahlung interactions have shown that RE due to Dreicer generation appear in the plasma center and subsequently drift outwards. Details on the local RE losses linked to MHD activity are provided by a Cherenkov probe.

Dedicated experiments on RE onset and suppression in FTU indicate that the measured threshold electric field for RE generation *(E_{thr})* is larger by a factor ~2-5 than expected according to the purely collisional theory; on the contrary, E_{thr} reasonably agrees with the new threshold calculated including synchrotron radiation losses. This confirms earlier results from FTU RE suppression experiments carried out in presence of electron-cyclotron heating [13]. Moreover, the theoretical dependence of the new threshold on the plasma parameters (B_T, Z_{eff} and n_e) is also matched reasonably well by the experimental data. These findings might imply a lower threshold density value to be achieved by means of massive gas injection for RE suppression in ITER. However, it is still an open question whether such results, that are obtained in the I_p flattop of ohmic plasmas, can be confirmed for disruption-generated RE.

Two algorithms for the *active control* of disruption-generated RE have been implemented in FTU: they redefine in real-time the external plasma radius (R_{ext}) and I_p ramp-down references, exploiting magnetic and gamma-ray signals. The I_p ramp-down is performed via the central solenoid and the current in the poloidal coils is changed to control the position of the RE beam as determined by the magnetic measurements. It has been shown that by means of a slow I_p ramp-down (~1MA/s up to 200 ms) and of a reduction of R_{ext} (approximately 10 % of the flat-top value), there are indications of RE beam energy suppression and reduced interactions with the vessel (especially in the low-field side), thus prompting *RE active control* as alternative/complementary technique to MGI. Further work is necessary to better refine the optimal R_{ext} reference during the RE beam I_p ramp-down, possibly defined as a function of I_p and RE beam energy. Moreover, the availability of real-time density profile from the scanning interferometer will allow to improve the estimate of the runaway beam radial position and enable more robust runaway beam suppression strategies. Future plans also include a re-design of the PID-T and PID-F current and position controllers, based on a RE beam dynamical model, to further improve their performances specifically in the RE control phase.

References

[1] Causa F et al. 2015, Cherenkov emission provides detailed picture of non-thermal electron dynamics in the presence of magnetic islands, *Nucl. Fusion* **55** 123021.

[2] Marocco D et al. 2015 First results on runaway electron studies using the FTU neutron camera, *Fusion Engineering and Design* **96–97**, 852.

[3] Tudisco O et al. 2004, Chapter 8: The diagnostic systems in the FTU, *Fusion Science and Technology* **45** 402.

[4] Bertalot L et al. 1992, Improved calibration of the neutron yield measurement system on the FTU tokamak, *Rev. Sci. Instrum* **63**, 4554.

[5] Esposito B et al. 2003, Dynamics of high energy runaway electrons in the Frascati Tokamak Upgrade, *Phys. Plasmas* **10** 2350.

[6] Batistoni P et al. 1995, Design of the neutron multicollimator for Frascati tokamak upgrade, *Rev. Sci. Instrum.* **66**, 4949.

[7] Riva M 2013, Real time n/γ discrimination for the JET neutron profile monitor, *Fusion Engineering and Design* **88**, 1178.
[8] Canton A, Innocente P and Tudisco O 2006, Two-color medium-infrared scanning interferometer for the Frascati tokamak upgrade fusion test device', *Applied Optics* **36**, 45.
[9] Boncagni L et al. 2016, MARTe real-time acquisition system of a Two-Color Interferometer for electron density measurements on FTU (Frascati tokamak upgrade), *Proc. 20th IEEE-NPSS Real-Time Conference*.
[10] Stahl A et al. 2013, Synchrotron radiation from a runaway electron distribution in tokamaks, *Phys. Plasmas* **20**, 093302.
[11] Popovic Z et al. 2016, On the measurement of the threshold electric field for runaway electron generation in the Frascati Tokamak Upgrade, to be submitted to *Phys. Plasmas*
[12] Connor J W and Hastie R J 1975, Relativistic limitations on runaway electrons, *Nucl. Fusion* **15** 415.
[13] Martin-Solis J R et al. 2010, Experimental Observation of Increased Threshold Electric Field for Runaway Generation due to Synchrotron Radiation Losses in the FTU Tokamak, *Phys. Rev. Lett.* **105** 185002.
[14] Granetz R et al. 2014, An ITPA joint experiment to study runaway electron generation and suppression, *Phys. Plasmas* **21** 072506.
[15] Lehnen M et al. 2015, Disruptions in ITER and strategies for their control and, *Journal of Nuclear Materials* **463** 39.
[16] Smith H M and Verwichte E 2008, Hot-tail runaway electron generation in tokamak disruptions, *Phys. Plasmas* **15**, 072502.
[17] Putvinski S 2010, Disruption Mitigation in ITER, *Proc. 23rd IAEA Fusion Conference*, Vol 43, ITR/1-6.
[18] Hollmann E et al. 2015, Status of research toward the ITER disruption mitigation system, *Phys. Plasmas* **22**, 021802.
[19] Esposito B et al. 2009, Disruption control on FTU and ASDEX upgrade with ECRH, *Nucl. Fus.* **49**, 065014.
[20] Lehnen M et al., 2008, Suppression of Runaway Electrons by Resonant Magnetic Perturbations in TEXTOR Disruptions, *Phys. Rev. Lett.* **100**, 255003.
[21] Papp G et al. 2011, Runaway electron losses enhanced by resonant magnetic perturbations, *Nucl. Fus.* **51**, 043004.
[22] Matsuyama A, Yagi M and Kagei Y 2013, Stochastic Transport of Runaway Electrons due to Low-order Perturbations in Tokamak Disruption, *Proceedings of the 12th Asia Pacific Physics Conference (APPC12)*, JPSCP.1.015037.
[23] Eidietis N W et al. 2012, Control of post-disruption runaway electron beams in DIII-D, *Phys. Plasmas* **19**, 056109.
[24] Lukash V et al. 2013, Study of ITER plasma position control during disruptions with formation of runaway electrons, *Proc. 40th EPS Conference on Plasma Physics*, P5.167.
[25] Snipes J A et al. 2014, Physics of the conceptual design of the ITER plasma control system, Fusion Engineering and Design **89**, 507.
[26] Vlainic M et al. 2015, Post-Disruptive Runaway Electron Beam in COMPASS Tokamak, *arXiv:1503.02947v1, physics.plasm-ph*.
[27] Saint-Laurent F et al. 2011, Control of Runaway Electron Beam Heat Loads on Tore Supra, *Proc. 38th EPS Conference on Plasma Physics*, O3.118.
[28] Hollmann E M et al. 2013, Control and dissipation of runaway electron beams created during rapid shutdown experiments in DIII-D, *Nucl. Fusion* **53**, 083004.
[29] Lehnen M et al. 2011, Disruption mitigation by massive gas injection in JET, *Nucl. Fusion* **51**, 123010.
[30] Boncagni L et al. 2014, An overview of the software architecture of the plasma position, current and density real-time controller of the FTU, *Fusion Engineering and Design* **89**, 204.
[31] Astolfi A et al. 2014, Adaptive hybrid observer of the plasma horizontal position at FTU, *Mediterranean Conference of Control and Automation*, 1088, (doi 10.1109/MED.2014.6961519).
[32] Ariola M and Pironti A 2008, Magnetic Control of Tokamak Plasmas, Springer, ISBN: 978-1-84800-323-1.
[33] Boncagni L et al. 2011, First steps in the FTU migration towards a modular and distributed real-time control architecture based on MARTe, *IEEE Transactions on Journal Nuclear Science* **58**, 1778.
[34] Boncagni L et al. 2012, MARTe at FTU: The new feedback control, *Fusion Engineering and Design* **87** 1917.
[35] Boncagni L et al. 2013, A first approach to runaway electron control in FTU, *Fusion Engineering and Design* **8**, 1109.
[36] Carnevale D et al. 2009, A new extremum seeking technique and its application to maximize RF heating on FTU, *Fusion Engineering and Design* **84**, 554.
[37] Carnevale D et al. 2008, Extremum seeking without external dithering and its application to plasma RF heating on FTU, *IEEE Conference on Decision and Control* 3151.

Ackonowledgements

This work was carried out within the framework of the EUROfusion Consortium and received funding from the Euratom research and training programme 2014-2018 under grant agreement No 633053 (Projects MST2-9 and MST2-15). The views and opinions expressed herein do not necessarily reflect those of the European Commission. Additional financial support was received from MINECO (Spain), Projects No. ENE2012-31753 and ENE2015-66444-R.